THE JOURNAL OF BIOLOGICAL CHEMISTRY VOL. 292, NO. 11, pp. 4457–4468, March 17, 2017

Novel Molecular Insights into the Catalytic Mechanism of Marine Bacterial Alginate Lyase AlyGC from Polysaccharide Lyase Family 6*

Received for publication, November 2, 2016, and in revised form, January 15, 2017 Published, JBC Papers in Press, February 1, 2017, DOI 10.1074/jbc.M116.766030

Fei Xu[‡], Fang Dong[‡], Peng Wang[‡], Hai-Yan Cao[‡], Chun-Yang Li[‡], Ping-Yi Li[‡], Xiu-Hua Pang[‡], Yu-Zhong Zhang[‡§], and Xiu-Lan Chen[‡1]

From the [‡]State Key Laboratory of Microbial Technology, Marine Biotechnology Research Center, Institute of Marine Science and Technology, Shandong University, Jinan 250100 and the [§]Laboratory for Marine Biology and Biotechnology, Qingdao National Laboratory for Marine Science and Technology, Qingdao 266000, China

Edited by F. Peter Guengerich

Alginate lyases that degrade alginate via a β-elimination reaction fall into seven polysaccharide lyase (PL) families. Although the structures and catalytic mechanisms of alginate lyases in the other PL families have been clarified, those in family PL6 have yet to be revealed. Here, the crystal structure of AlyGC, a PL6 alginate lyase from marine bacterium *Glaciecola chathamensis* S18K6^T, was solved, and its catalytic mechanism was illustrated. AlyGC is a homodimeric enzyme and adopts a structure distinct from other alginate lyases. Each monomer contains a catalytic N-terminal domain and a functionally unknown C-terminal domain. A combined structural and mutational analysis using the structures of AlyGC and of an inactive mutant R241A in complex with an alginate tetrasaccharide indicates that conformational changes occur in AlyGC when a substrate is bound and that the two active centers in AlyGC may not bind substrates simultaneously. The C-terminal domain is shown to be essential for the dimerization and the catalytic activity of AlyGC. Residues Tyr^{130}, Arg^{187}, His^{242}, Arg^{265}, and Tyr^{304} in the active center are also important for the activity of AlyGC. In catalysis, Lys^{220} and Arg^{241} function as the Brønsted base and acid, respectively, and a Ca^{2+} in the active center neutralizes the negative charge of the C5 carboxyl group of the substrate. Finally, based on our data, we propose a metal ion-assisted catalytic mechanism of AlyGC for alginate cleavage with a state change mode, which provides a better understanding for polysaccharide lyases and alginate degradation.

Brown algae are an important source of primary production in the marine eco-system and represent a huge marine biomass (1). Alginates are the major polysaccharides produced by brown alga, which may reach 40% of the dry weight of algal biomass (2). Alginate is a linear polysaccharide composed of α-L-guluronate (G)[2] and its C5 epimer β-D-mannuronate (M), which are arranged in three ways, polyguluronate (PG), polymannuronate (PM), and alternating GM or random heteropolymeric M/G stretches (P(MG)) (3). Alginates are widely used in the food, chemical, and pharmaceutical industries because of their ability to form gels and to chelate metal ions (4–6). In addition, alginates are also a major constituent of biofilm produced by some heterotrophic bacteria from the genera *Pseudomonas* and *Azotobacter* (7). Alginate lyases are synthesized by brown seaweeds, marine molluscs, and a variety of microbes (8). They play an important role in the marine carbon cycle and have important applications in biotechnological and chemotherapeutic fields, such as preparation of functional oligosaccharides (9) and protoplasts of algae (10) and treatment of cystic fibrosis (11, 12). With the discovery and characterization of novel enzymes, further applications of alginate lyases may be found. Alginate lyases degrade alginates through a β-elimination reaction, targeting the glycosidic 1→4 *O*-linkage between the monomers. A double bond is formed between C4 and C5, yielding a 4-deoxy-L-*erythro*-hex-4-enopyranosyluronic acid at the nonreducing end (13). According to their substrate specificities, alginate lyases are classified into three types, PM-specific lyases (EC 4.2.2.3), PG-specific lyases (EC 4.2.2.11), and bifunctional lyases that can degrade both PM and PG (EC 4.2.2.-). Most alginate lyases studied are endolytic enzymes that cleave glycosidic bonds inside polymers and release unsaturated oligosaccharides, and only a few exolytic alginate lyases that remove monomers or dimers from the ends of polymers are reported (14–17). In the Carbohydrate-Active enZYmes database (CAZY database), alginate lyases are distributed in seven polysaccharide lyase (PL) families (PL5, -6, -7, -14, -15, -17, and -18) (18). Whereas those of alginate lyases from PL5, -7, -14, -15, -17, and -18 have been reported, the three-dimensional structures and catalytic mechanisms of the PL6 alginate lyases still remain unknown (7, 15, 19–22). Clarifying the structure and catalytic

* This work was supported by National Science Foundation of China Grants 31290230, 31290231, 41676180, and 31670038, Program of Shandong for Taishan Scholars Grant TS20090803, and National Postdoctoral Program for Innovative Talents Grant BX201600095. The authors declare that they have no conflicts of interest with the contents of this article.
The atomic coordinates and structure factors (codes 5GKD and 5GKQ) have been deposited in the Protein Data Bank (http://wwpdb.org/).
[1] To whom correspondence should be addressed. Tel.: 86-531-88365013; Fax: 86-531-88564326; E-mail: cxl0423@sdu.edu.cn.

[2] The abbreviations used are: G, α-L-guluronate; PL, polysaccharide lyase; M, β-D-mannuronate; NTD, N-terminal domain; CTD, C-terminal domain; PDB, Protein Data Bank; TBA, thiobarbituric acid; r.m.s.d., root mean square deviation; M4, D-tetramannuronic acid tetrasodium salt; DLS, dynamic light scattering; DS, dermatan sulfate; PG, polyguluronate; PM, polymannuronate.

mechanism of the PL6 alginate lyases will broaden our understanding on alginate lyases.

In the PL6 family, only three alginate lyases have been characterized (23–25). AlyMG (475 amino acid residues) is a polyMG-specific alginate lyase from *Stenotrophomas maltophilia* KJ-2 (24). AlyP (398 amino acid residues) from *Pseudomonas* sp. OS-ALG-9 has a greater specificity to PM than to PG (23). OalS6 (named AlgS6 in the NCBI Protein Database, but changed to OalS6 when published) (770 amino acid residues) from *Shewanella* sp. Kz7 is an exo-type oligoalginate lyase that prefers to depolymerize the PG block (25). In addition to alginate lyases, the PL6 family also contains a chondroitinase B (ChonB, also named CslB) (506 amino acid residues) from *Pedobacter heparinus*. ChonB is a glycosaminoglycan (GAG) lyase with disaccharide polymer dermatan sulfate (DS) as its sole substrate. ChonB adopts a right-handed β-helix fold and has a calcium-dependent catalytic machinery (26, 27).

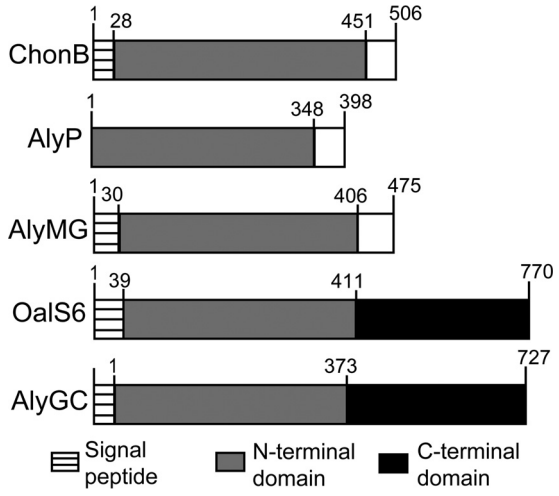

FIGURE 1. **Schematic domain diagram of PL6 enzymes.** The signal peptides were predicted by SignalP 4.1 Server. ChonB (GenBank™ ACU03011.1; PDB code 1DBG) is from *P. heparinus* DSM 2366; AlyP (GenBank™ BAA01182.1) is from *Pseudomonas* sp. OS-ALG-9; AlyMG (GenBank™ AFC88009.1) is from *S. maltophilia* KJ-2; OalS6 (GenBank™ AHC69713.1) is from *Shewanella* sp. Kz7, and AlyGC (GenBank™ BAEM00000000.1) is from *Glaciecola chathamensis* S18K6^T.

In this study, a PL6 alginate lyase, AlyGC, from marine bacterium *Glaciecola chathamensis* S18K6^T (28, 29) was characterized, and the structures of wild-type (WT) AlyGC (2.2 Å resolution) and of an inactive mutant in complex with an alginate tetrasaccharide (2.6 Å resolution) were solved. Based on structural and mutational analyses, the molecular mechanism of AlyGC for substrate catalysis was explained. The results provide a better understanding of the PL6 alginate lyases.

Results and Discussion

Two-domain Structure of AlyGC Predicted by Sequence Analysis—The gene *alyGC* predicted to encode a PL6 alginate lyase (AlyGC) was cloned from the genome of *G. chathamensis* S18K6^T. *alyGC* is 2265 bp in length and encodes a protein of 754 amino acid residues containing a predicted 28-residue signal peptide. According to the blast result against the NCBI non-redundant protein database, the putative protein AlyGC (unless otherwise stated, AlyGC discussed hereafter is 727 aa in length without the predicted signal peptide) shows the highest identity (58%) to OalS6, a characterized PL6 alginate lyase from *Shewanella* sp. Kz7 (25). Sequence analysis using Conserved

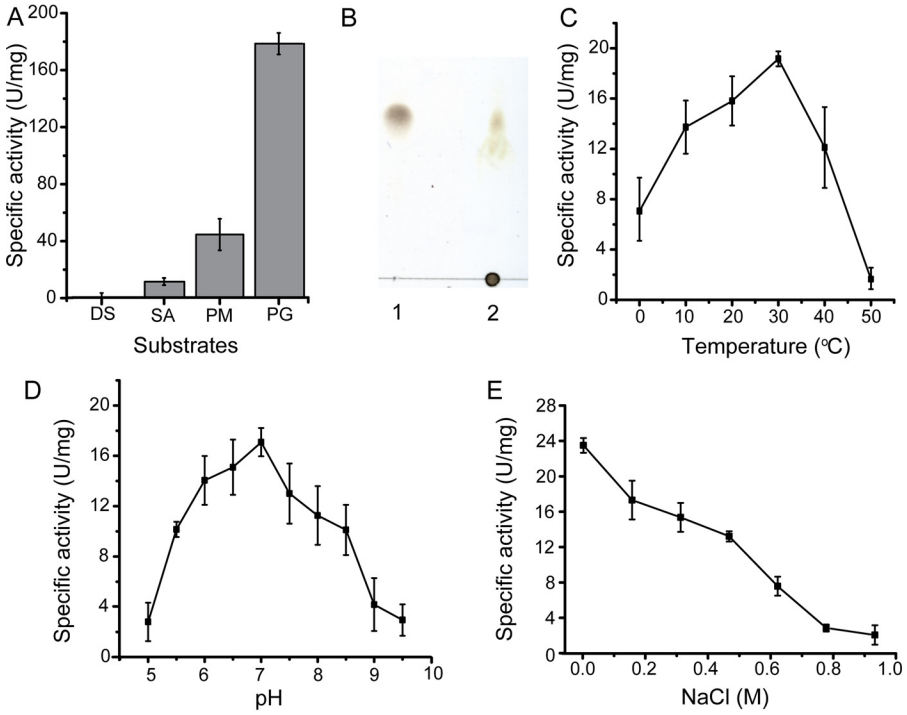

FIGURE 2. **Biochemical characterization of AlyGC.** *A,* substrate specificities of AlyGC toward dermatan sulfate (*DS*), sodium alginate (*SA*), polymannuronate (*PM*), and polyguluronate (*PG*). Experiments were conducted in a 200-μl mixture containing 25 μg/ml enzyme and 2 mg/ml substrate in 50 mM Tris-HCl (pH 7.5) at 30 °C for 30 min. *B,* TLC analysis of the degradation products of AlyGC on PG. A 200-μl reaction mixture containing 50 μg/ml enzyme and 2 mg/ml PG was incubated at 30 °C for 3 h. *Lane 1,* monoguluronic acid standard; *lane 2,* the degradation products from PG by AlyGC. *C,* effect of temperature on AlyGC activity. *D,* effect of pH on AlyGC activity. Experiments were performed at 30 °C in 50 mM Britton-Robinson buffer ranging from pH 5 to 9.5. *E,* effect of salinity on AlyGC activity. Assays in *C–E* were carried out with sodium alginate as the substrate.

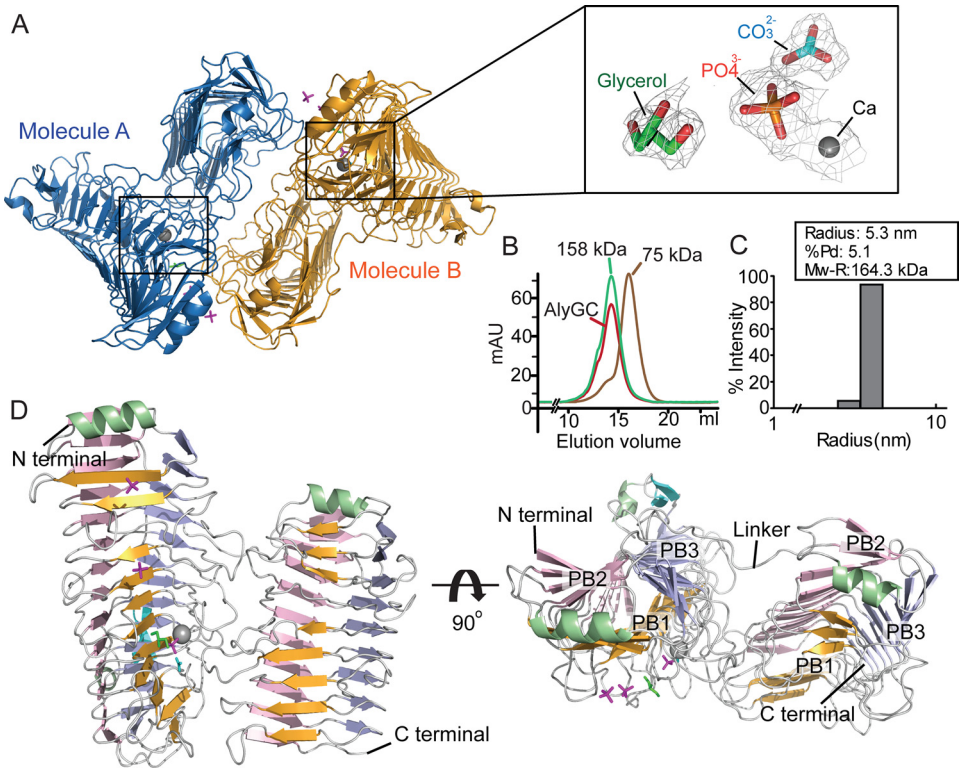

FIGURE 3. **Overall structure of AlyGC.** *A,* structure of dimeric AlyGC in one asymmetric unit. $2F_o - F_c$ omit electron density (1.0 σ) of the Ca^{2+} and of the molecules bound beside it is *boxed*. *B,* gel filtration analysis of the form of AlyGC in solution using aldolase (158 kDa) and conalbumin (75 kDa) as protein size standards. *C,* DLS analysis of the molecular weight of AlyGC. *D*, overall structure of AlyGC monomer. PB1, PB2, and PB3 are colored in *orange, pink,* and *pale cyan*, respectively. α-Helix is colored in *pale green*.

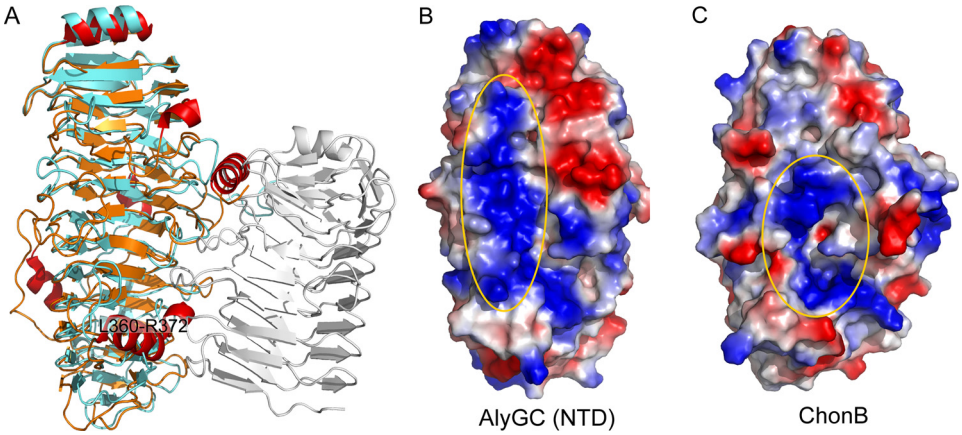

FIGURE 4. **Structural comparison of AlyGC and ChonB.** *A,* structural alignment of AlyGC and ChonB. The NTD and the linker of AlyGC are colored in *cyan*, and the CTD of AlyGC is colored in *gray*. ChonB is shown in *orange* schematic view, the α-helices of which are colored in *red*. *B* and *C,* electrostatic surface views of the NTD of AlyGC (*B*) and ChonB (*C*). The catalytic clefts are *circled*.

Domain Search suggests that AlyGC contains two domains, an N-terminal domain (NTD, Met^1–Asn^{373}) and a C-terminal domain (CTD, Gln^{374}–Leu^{727}). The NTD of AlyGC belongs to the PL6 family; however, the CTD of AlyGC does not display obvious similarity to any known functional protein sequences. Although not reported, sequence analysis indicates that the precursor of alginate lyase OalS6 also has a similar CTD with unidentified function (Fig. 1). Thus, these two CTDs may represent an uncharacterized protein domain. Taken together, sequence analysis indicates that AlyGC is a PL6 alginate lyase with a two-domain structure.

Characterization of AlyGC—AlyGC without the predicted signal peptide was overexpressed in *Escherichia coli*. Because AlyGC is a member of the PL6 family that contains alginate lyase and chondroitinase B, the activities of recombinant AlyGC toward alginate sodium and DS were measured. AlyGC showed activity toward alginate sodium but no detectable activity toward DS (Fig. 2*A*), indicating that AlyGC is an alginate lyase, rather than a GAG lyase. Among alginate sodium, PM and PG, AlyGC displayed the highest activity toward PG, indicating its preference to PG (Fig. 2*A*). Thin layer chromatography (TLC) analysis showed that AlyGC released monosaccha-

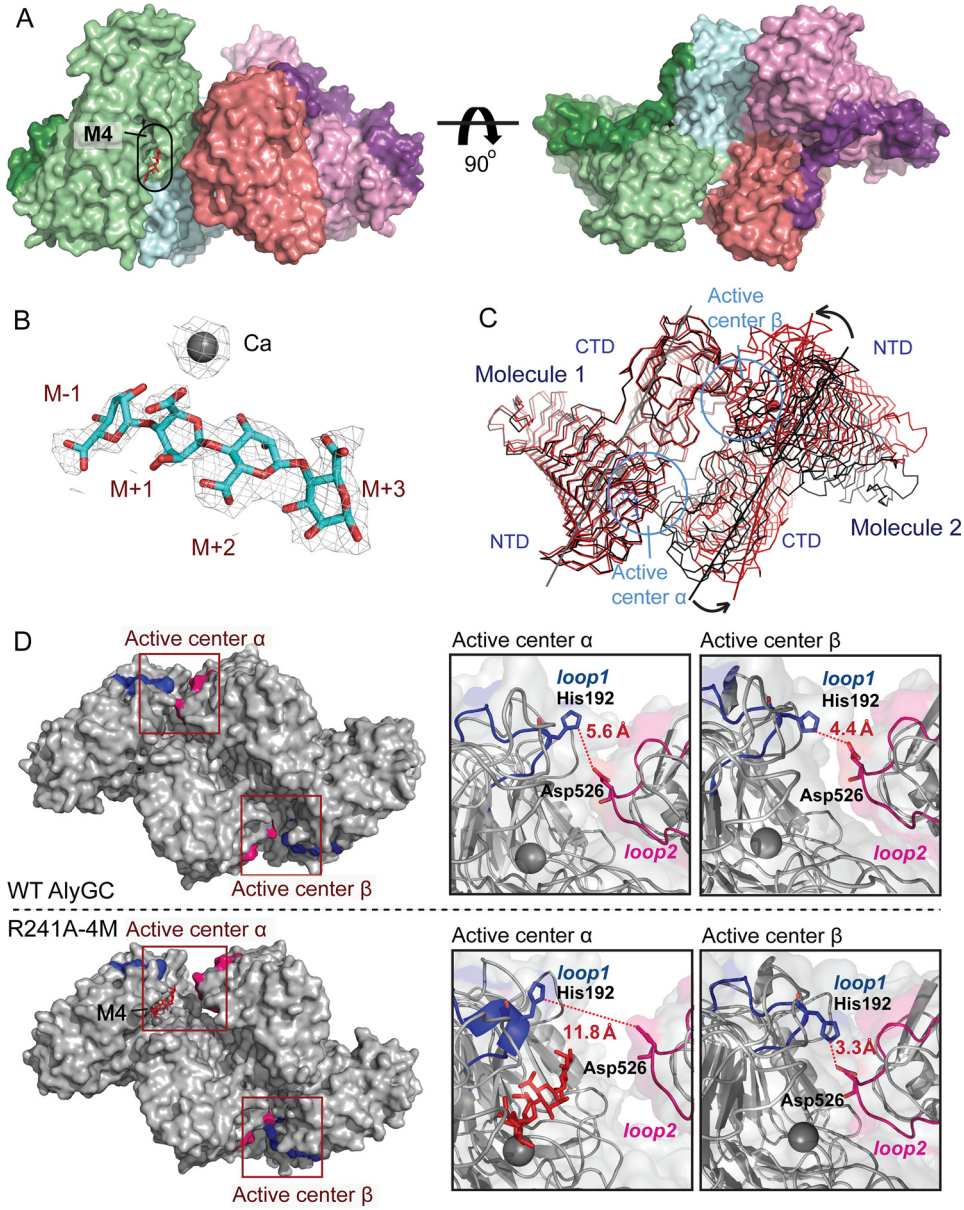

FIGURE 5. **Structure of R241A-tetrasaccharide complex.** *A,* surface representation of R241A-tetrasaccharide complex dimer. The NTD, linker, and CTD of one molecule are colored in *pale green*, *dark green*, and *blue,* respectively, and those of another molecule are colored in *pink, purple,* and *red*, respectively. The substrate, M4, is shown as *red sticks*. *B,* $2F_o - F_c$ omit electron density (1.0 σ) of the Ca^{2+} (*gray ball*) and M4 (*blue stick*) in the active center. *C, ribbon* representation of conformational changes between structures of WT AlyGC dimer (*black*) and R241A-M4 dimer (*red*). Molecule 1 in R241A-M4 dimer is aligned to molecule 1 in WT AlyGC dimer. The *lines* in each molecule were connected between Asn^{44} and Ala^{466}. *D,* distances (*dotted lines*) between His^{192} on loop 1 (Ile^{188}–Leu^{201}, colored in *blue*) of the NTD and Asp^{526} on loop 2 (Asp^{520}–Ile^{533}, colored in *pink*) of the CTD in WT AlyGC (up) and R241A-M4 (down).

rides from PG (Fig. 2*B*), indicating that AlyGC is an exo-type lyase, consistent with that reported for OalS6 (25). With alginate sodium as substrate, AlyGC exhibited the highest activity at 30 °C and pH 7.0 (Fig. 2, *C* and *D*). Although from a marine bacterium, AlyGC showed very low level of salt tolerance (Fig. 2*E*).

Overall Structure of AlyGC—A similarity search at Protein Data Bank (PDB) revealed that the closest homologue to AlyGC is ChonB (PDB code 1DBG), with 29% sequence identity (covering only 46% of the AlyGC sequence), which indicates that no suitable structure model can be used for AlyGC structure construction. Therefore, to solve the structure of AlyGC, the crystals of both WT AlyGC and SeMet-AlyGC were obtained. Then HKL2MAP was used for heavy atom searching, and Phenix. autosol was used for phasing and density modification. The values of the figure of merit (FOM) and BAYES-CC of the phasing result are 0.348 and 39.88, respectively. Finally, combined with the data of WT AlyGC, the structure of AlyGC was solved at 2.2 Å resolution. The AlyGC structure belongs to the *P*21 space group. Four AlyGC molecules (each contains 727 residues) are found in one asymmetric unit. Only two of the four have interactions (Fig. 3*A*), and the other two do not show the same symmetry-related interaction. In addition, both gel filtration and dynamic light scattering (DLS) analyses indicate that AlyGC presents as dimers in solution (Fig. 3, *B* and *C*). Therefore, AlyGC is a dimeric enzyme. The electron density of AlyGC

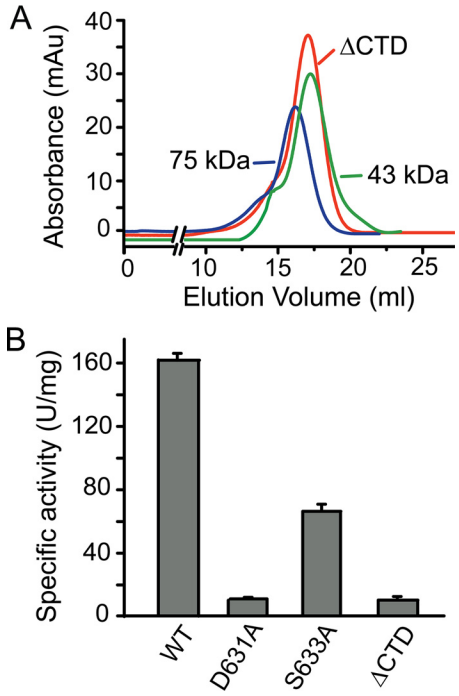

FIGURE 6. **Functional analysis of the CTD.** *A*, gel filtration analysis of the form of ΔCTD in solution using conalbumin (75 kDa) and ovalbumin (43 kDa) as protein size standards. *B*, enzymatic activities of AlyGC mutants toward PG.

crystal indicates that one metal ion is located in the center of the NTD of each AlyGC monomer, which is confirmed to be Ca^{2+} via inductively coupled plasma, optical emission spectrometry (ICP-OES) analysis. A carbonate ion, a phosphate ion, and a glycerol molecule, which are most likely from the crystallization buffer, are bound near the Ca^{2+} (Fig. 3*A*). In addition, another two phosphate ions are also found in AlyGC structure.

The NTD (Met^{1}–Lys^{408}) and the CTD (His^{442}–Leu^{727}) in an AlyGC monomer form a "twin tower-like" shape in the front view (Fig. 3*D*), which, however, intersects at an angle (Fig. 3*A*). The NTD and the CTD both adopt right-handed parallel β-helix folds, which are connected by a linker (Ala^{387}–Lys^{441}) (Fig. 3*D*). In an AlyGC dimer, two monomers are centrosymmetric. The two CTDs are nearly parallel, and the two NTDs point outside in opposite directions (Fig. 3*A*). Most of the interface between the two monomers occurs between the CTDs. In addition, some residues of the NTD of one monomer have interactions with the residues of the CTD of another monomer. Right-handed β-helix folds are common in pectate lyases from PL1, PL3, and PL9 and DS lyases from PL6. However, these lyases contain only one β-helix domain (27, 30–32). According to previous nomenclature (33, 34), the three parallel β-sheets in this fold are referred to as PB1, PB2, and PB3, and the turns or loops between two β-sheets are referred to as T1 (between PB1 and PB2), T2 (between PB2 and PB3), and T3 (between PB3 and PB1). One coil refers to the regular three-stranded parallel β-helical structure that starts with PB1 and ends with PB3, and therefore, the arrangement of one coil of the parallel β-helix is PB1-T1-PB2-T2-PB3-T3. Most conserved residues are located in the T3-PB1-T1 region (34). In the cross-sectional view of AlyGC β-helix, PB1 and PB2 are nearly antiparallel, and PB3 is almost perpendicular to PB2. The NTD consists of 12 coils starting with the first PB1 strand (Glu^{36}–Lys^{42}) and finishing with the penultimate PB3 strand (Asn^{370}–Asn^{373}), which includes 12 PB1 strands, 14 PB2 strands, and 14 PB3 strands. The CTD consists of eight coils starting with the first PB1′ strand (Leu^{478}–Leu^{480}) and finishing with the penultimate PB3′ strand (Val^{699}–Glu^{701}), which includes 9 PB1′ strands, 11 PB2′ strands, and 9 PB3′ strands. There are only two α-helices in the structure of AlyGC, designated HA1 and HA2. The NTD is capped by HA1 (Pro^{9}–Lys^{18}) preceding the first PB1 strand and the CTD by HA2 (Thr^{451}–Ser^{458}) preceding the first PB1′ strand. The linker between the NTD and the CTD consists of two β-strands followed by a long loop of 42 residues. The Ca^{2+} is located in the T3-PB1-T1 region of coils 6 and 7 in the NTD.

A structure-based homology search for AlyGC was performed using the DALI server (35). The result indicates that ChonB is the closest structural homologue with a Z-score of 39.7 and a root mean square deviation (r.m.s.d.) of 2.3 on 395 aligned Cα residues. Other structural homologues include the mannuronan C5 epimerase AlgE4 from *Azotobacter vinelandii* (PDB code 2PYG; Z-score: 28.4, and r.m.s.d.: 2.8 on 310 residues) (36) and the K5 lyase from *Escherichia* virus k1–5 (PDB code 2X3H; Z-score: 26.6, and r.m.s.d.: 2.8 on 301 residues) (37). AlyGC exhibits similar topology with these proteins. However, these homologues adopt single right-handed parallel β-helix folds, whereas AlyGC adopts a tandem β-helix fold. ChonB has an α-helix (Leu^{360}–Arg^{372}) in the catalytic cleft, which, however, is lacking AlyGC. Because this α-helix in ChonB is an important component of the catalytic cleft and residue Arg^{363} on this α-helix directly interacts with the substrate DS (26, 27), this structural difference between ChonB and AlyGC may be related to their different substrate specificity (Fig. 4*A*). In addition, the catalytic cleft of ChonB is more L-like compared with that of AlyGC (Fig. 4, *B* and *C*).

Conformational Change in AlyGC When Binding an Alginate Tetrasaccharide—To obtain an inactive AlyGC mutant for enzyme-substrate complex crystallization, site-directed mutations on AlyGC were conducted based on structural analysis. The result indicated that when Lys^{220} or Arg^{241} was mutated to alanine, the mutated AlyGC was almost inactive (<5% activity of WT AlyGC) toward PG. Thus, mutants K220A and R241A were crystallized with alginate oligosaccharides, respectively. Finally, the crystal structure of R241A in complex with tetramannuronic acid (M4) was solved to 2.6 Å resolution. There are two R241A molecules in one asymmetric unit of the crystal structure R241A-M4, each containing a Ca^{2+} (Fig. 5*A*). Of the two active centers (α and β) in the dimeric R241A-M4, only the active center α binds an M4 beside the Ca^{2+} (Fig. 5*B*). Structural comparison of R241A-M4 and WT AlyGC indicates that conformational changes occur in the R241A-M4 dimer (Fig. 5*C*). Compared with WT AlyGC, the entrance of the active center α that binds the M4 is enlarged and that of the active center β without substrate is smaller. To characterize this, we compared the closest distances between two loops (1 and 2) at the entrances of the catalytic clefts in WT AlyGC and R241A-M4. Loop 1 (Ile^{188}–Leu^{201}) is from the NTD of one monomer, and loop 2 (Asp^{520}–Ile^{533}) is from the CTD of another monomer. The closest distance between loops 1 and 2 is that between His^{192} and Asp^{526} in AlyGC structures. In WT AlyGC, the dis-

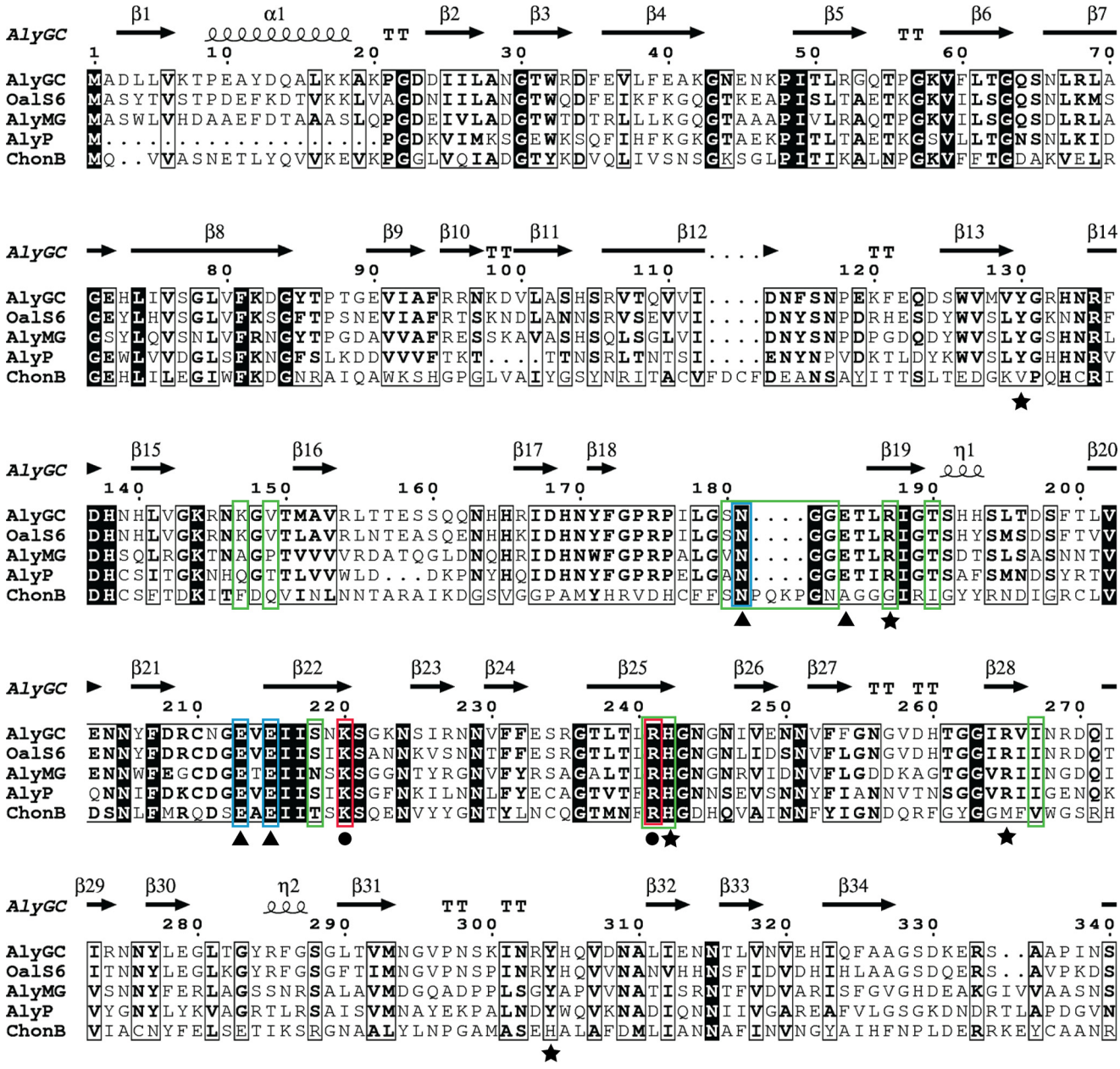

FIGURE 7. **Sequence alignment of AlyGC with the characterized PL6 enzymes.** α-Helices and β-strands are represented as *loops* and *arrows*, respectively, and β-turns are marked with *TT*. AlyGC (GenBank™ BAEM00000000.1) from *G. chathamensis* S18K6^T, OalS6 (AHC69713.1) from *Shewanella* sp. Kz7, AlyMG (GenBank™ AFC88009.1) from *S. maltophilia* KJ-2, AlyP (GenBank™ BAA01182.1) from *Pseudomonas* sp. OS-ALG-9, and ChonB (GenBank™ ACU03011.1; PDB code 1DBG) from *P. heparinus* DSM 2366 are shown. The signal peptides of all the sequences predicted by SignalP 4.1 server are not included. *Dark shaded boxes* enclose conserved positions, and *light shaded boxes* show positions with homologous residues. The figure was prepared using ESPript program. Aligned with ChonB, residues that may be involved in the binding of substrate and Ca^{2+} and in catalysis are *boxed* in *green, blue,* and *red*, respectively. Residues in AlyGC, which are verified for the enzymatic activity, Ca^{2+} coordination, and catalysis, are shown in *stars*, *triangle* and *dots,* respectively.

tance between His^{192} and Asp^{526} near the active center α (5.6 Å) is similar to that near the active center β (4.4 Å). However, in R241A-M4, the distance between His^{192} and Asp^{526} near the active center α is significantly increased to 11.8 Å and that near the active center β is decreased to 3.3 Å (Fig. 5*D*), much smaller than the diameter of a carbohydrate chain. Therefore, based on the crystal structure of R241A-M4, it seems that the dimeric AlyGC can only accommodate one substrate molecule in one of the two active centers, although we cannot ensure that it is this case when AlyGC catalyzes substrates in solution.

Function of the CTD—The CTD in AlyGC has no conserved sequence or predicted function. To investigate the role of the CTD, a CTD-truncated mutation of AlyGC, ΔCTD (Met^1–Asp^{434}), was constructed. Gel filtration analysis showed that ΔCTD presents as monomers in solution (Fig. 6*A*), indicating that the CTD is essential for the dimerization of AlyGC. Compared with WT AlyGC, ΔCTD lost 94.3% activity toward PG (Fig. 6*B*), suggesting that, for AlyGC activity, the CTD is indispensable, and the dimerization of AlyGC is also necessary. Structural analysis shows that a loop from the CTD (Arg^{627}–His^{638}) stretches into the catalytic center. Mutations of the residues Asp^{631} and Ser^{633} on this loop to alanines led to significant decreases in the enzyme activity (Fig. 6*B*). Altogether, our data indicate that the CTD of

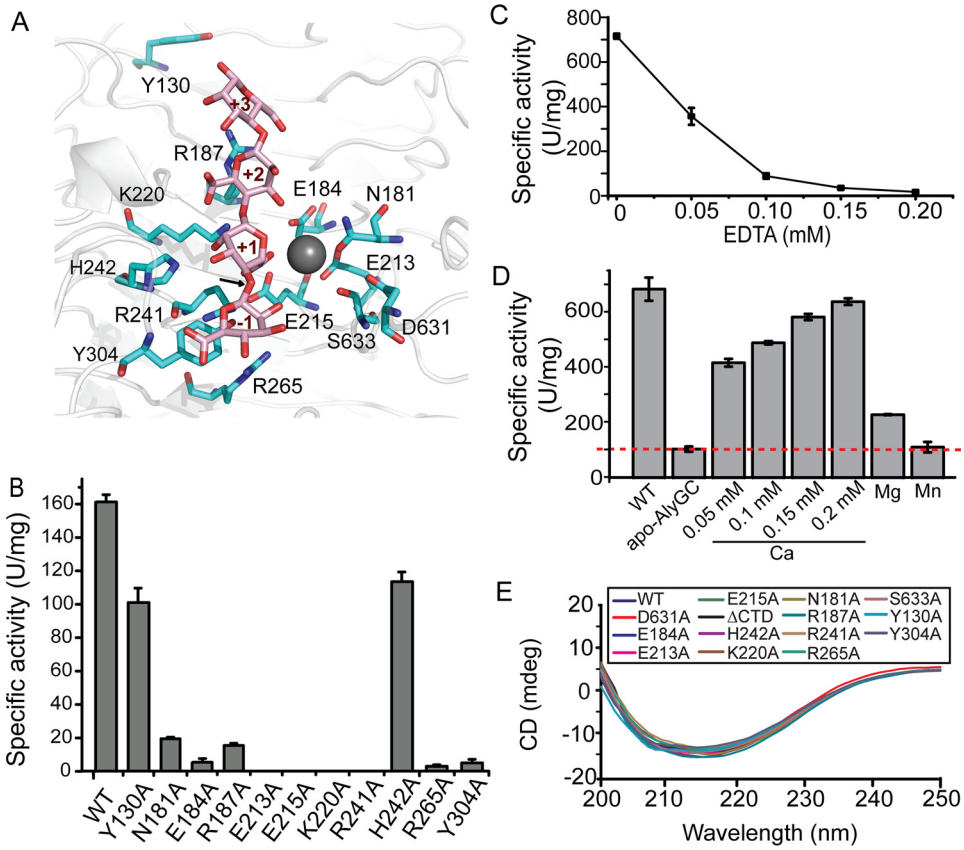

FIGURE 8. **Analyses of important amino acid residues in the active center of AlyGC.** *A,* residues interacting with M4 in R241A-M4. The side chain of Arg^{241} was modeled into the active site based on its location in the WT structure. The residues are presented as *blue sticks*, and the bound M4 from −1 to +3 subsites is shown as *pink sticks*. Ca^{2+} is shown as a *gray ball*. The cleavage site is indicated by an *arrow*. *B,* enzymatic activities of AlyGC mutants toward PG. *C,* effect of EDTA on the activity of AlyGC. *D,* effect of metal ions on the activity of apo-AlyGC. Enzyme activities in *C* and *D* were determined by measuring the absorbance at 548 nm with the TBA method (43). *E,* CD spectra of AlyGC and its mutants.

AlyGC is essential for the dimerization and the catalytic activity of AlyGC.

Role of the Ca^{2+} in Catalysis—ChonB, the only enzyme with a solved structure in PL6 family, contains a Ca^{2+} coordinated by Asn^{213}, Glu^{243}, and Glu^{245} (26, 27). The Ca^{2+} in AlyGC is coordinated by Asn^{181}, Glu^{213}, Glu^{215}, and Glu^{184}, all of which are conserved in the characterized PL6 alginate lyases (Figs. 7 and 8*A*). Among these residues, Asn^{181}, Glu^{213}, and Glu^{215} correspond to the coordinative residues of Ca^{2+} in ChonB (Fig. 7). In the R241A-M4 complex structure, the Ca^{2+} also interacts with the carboxyl group of the substrate. These structural data suggest that the Ca^{2+} in AlyGC may be involved in catalysis, just as that in ChonB (26). To support this, we performed site-directed mutations on the residues coordinating the Ca^{2+}. Substitution of any of the four residues to alanine resulted in severe loss in enzymatic activity (Fig. 8*B*). Furthermore, when metal chelator EDTA was added to the reaction mixture, the enzyme activity decreased with the increase of EDTA concentration, and 0.2 mM EDTA completely abolished the enzyme activity (Fig. 8*C*). However, the activity of apo-AlyGC in which the Ca^{2+} was completely depleted by EDTA could be recovered by the addition of Ca^{2+} and almost fully recovered by 0.2 mM Ca^{2+}. In contrast, Mg^{2+} could only recover 33.4% of the enzyme activity, and Mn^{2+} had no effect on the recovery of apo-AlyGC activity (Fig. 8*D*). Taken together, these data indicate that the Ca^{2+} in AlyGC is the biological metal ion and is involved in catalysis.

Important Residues in the NTD for Substrate Catalysis—The oligosaccharide is bound in the active center α of AlyGC as shown in Fig. 5 and mainly interacts with the T1-PB1-T3 region of the NTD. One end of the catalytic groove of AlyGC is nearly blocked, suggesting that AlyGC is an exo-type lyase, corresponding to the TLC result (Fig. 2*B*). We adopt the nomenclature proposed by Davies *et al.* (38) by convention. $-n$ and $+n$ represent the nonreducing terminus and the reducing terminus, respectively, and subsites are labeled from $-n$ to $+n$. Therefore, the tetrasaccharide binding to AlyGC is positioned at subsites −1, +1, +2, and +3, and the constituent mannuronate residues are named from M−1 to M+3. As shown in Fig. 8*A*, Arg^{241} is modeled in R241A-M4 structure according to the location of Arg^{241} in the WT AlyGC structure. In the structure of R241A-M4, Lys^{220} adjoins to the Cα of M+1, having the ability to donate electron. Arg^{241} is adjacent to the glycosidic bond between M−1 and M+1, able to accept electron. Both Lys^{220} and Arg^{241} are highly conserved in PL6 alginate lyases (Fig. 7). Mutation of Lys^{220} or Arg^{241} to alanine led to complete loss of the enzyme activity (Fig. 8*B*). Therefore, according to these data and the mechanism of β-elimination reaction, Lys^{220} is the Brønsted base, and Arg^{241} is the Brønsted acid in the cleavage reaction

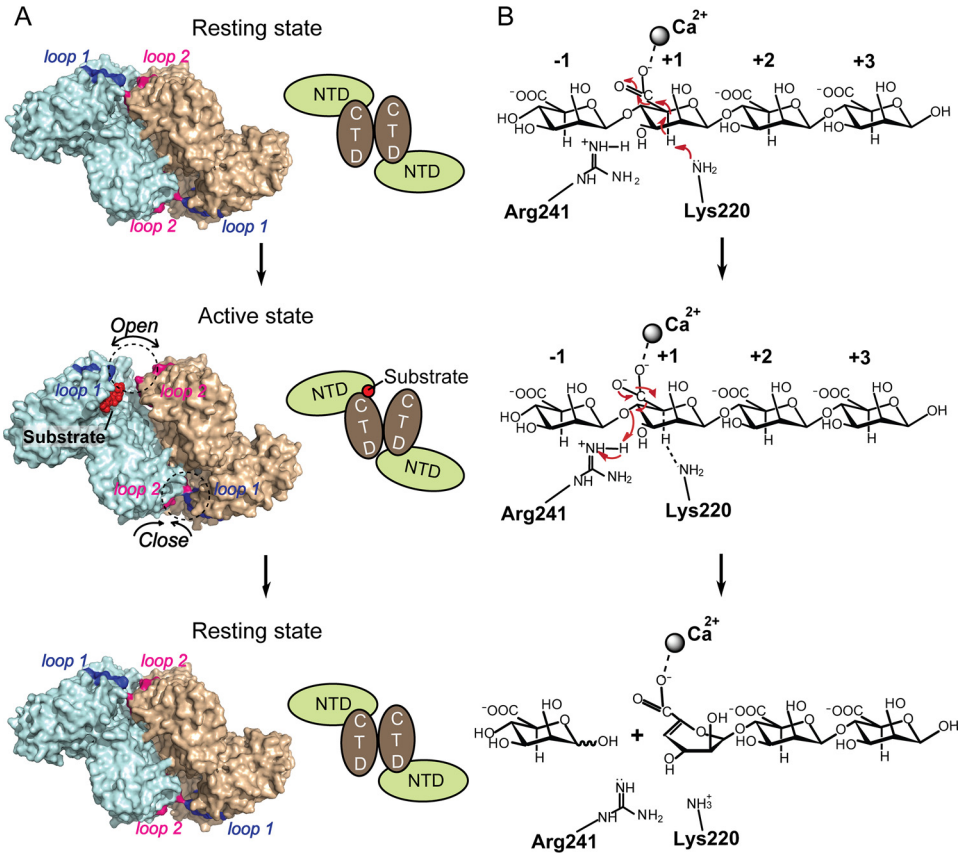

FIGURE 9. **Catalytic mechanism of AlyGC.** *A,* model of the catalytic mode of AlyGC. Step 1, the resting state. In the absence of substrate, the sizes of the entrances of the two active centers of AlyGC are similar. The whole enzyme is presented as surface view with one monomer colored in *pale cyan* and another in *wheat*. Loop 1 is colored in *dark blue,* and the loop 2 is colored in *pink*. A schematic diagram is presented on the right. Step 2, the active state. A substrate enters one of the catalytic cavities. The active center binding the substrate is enlarged, and the other one is smaller. The enzyme is in the active state. The substrate is shown as a *red sphere* in the right schematic diagram. Step 3, return to the resting state. The product is released and the enzyme molecule returns to the resting state. *B,* catalytic mechanism of AlyGC on alginate degradation. The Ca^{2+} forms interactions with the carboxyl group of the A+1 and activates the Cα hydrogen of A+1. Lys^{220} functions as a nucleophilic base to attack the Cα of A+1, and Arg^{241} functions as the Brønsted acid to accept an electron. Electron transfer is presented with *red arrows*.

of AlyGC on alginate, just as the corresponding residues in ChonB (26).

According to the WT AlyGC and R241A-M4 structures, the hydrophilic residues Tyr^{130}, Arg^{187}, His^{242}, Arg^{265}, and Tyr^{304} in the active center (Fig. 8*A*) may interact with the substrate. Residues Tyr^{130}, Arg^{187}, Arg^{265}, and Tyr^{304} are conserved in all characterized PL6 alginate lyases, and His^{242} is conserved in all characterized PL6 enzymes, including ChonB (Fig. 7). Site-directed mutations of these residues to alanine decreased the activity of AlyGC (Fig. 8*B*). These data indicate that these hydrophilic residues are important for the activity of AlyGC.

Circular dichroism (CD) spectra show that the curves of all the variants are similar to that of WT AlyGC, suggesting that WT AlyGC and the variants have similar secondary structures. Therefore, the activity loss in the variants is caused by amino acid replacement, rather than by structural change (Fig. 8*E*).

Catalytic Mechanism of AlyGC—Based on our structural and biochemical results on AlyGC, we propose a metal ion-assisted mechanism of this PL6 alginate lyase for alginate cleavage with a possible state change. In the absence of alginate, AlyGC is in the resting state, in which the sizes of the entrances of the two active centers are similar (Fig. 9*A*). When alginate or an oligosaccharide enters one of the catalytic cavities, the active center binding the substrate is enlarged and the other one is smaller. The enzyme is in the active state (Fig. 9*A*). The substrate is bound in the right position via the electrostatic interactions between the substrate and the hydrophilic residues in the active center. Then, the Ca^{2+} interacts with the carboxyl group of the A+1 (A represents a mannuronic acid or a guluronic acid), and activates the Cα hydrogen of A+1. Lys^{220} functions as the nucleophilic base to attack the Cα of A+1 (Fig. 9*B*), leading to the formation of an unstable substrate-AlyGC intermediate, in which both the Cα–H bond and the Cβ–O bond between A−1 and A+1 are weakened (Fig. 9*B*). Along with the formation of the N-H bond of Lys^{220} in AlyGC, the α-H of the substrate is released, and the Cβ–O bond between A−1 and A+1 is polarized and broken immediately (Fig. 9*B*). In this model, Arg^{241} functions as the Brønsted acid to accept electron and helps to cleave the Cβ–O bond. After that, the product is released, and AlyGC is back to the resting state, ready to catalyze the cleavage of another substrate (Fig. 9*A*).

Structure and Catalytic Mechanism Comparison of Alginate Lyases—Alginate lyases fall into seven PL families, including PL5-7, -14, -15, -17, and -18 (18). With the three-dimensional structures of WT AlyGC and its complex being solved, at least one alginate lyase structure has been revealed in each family

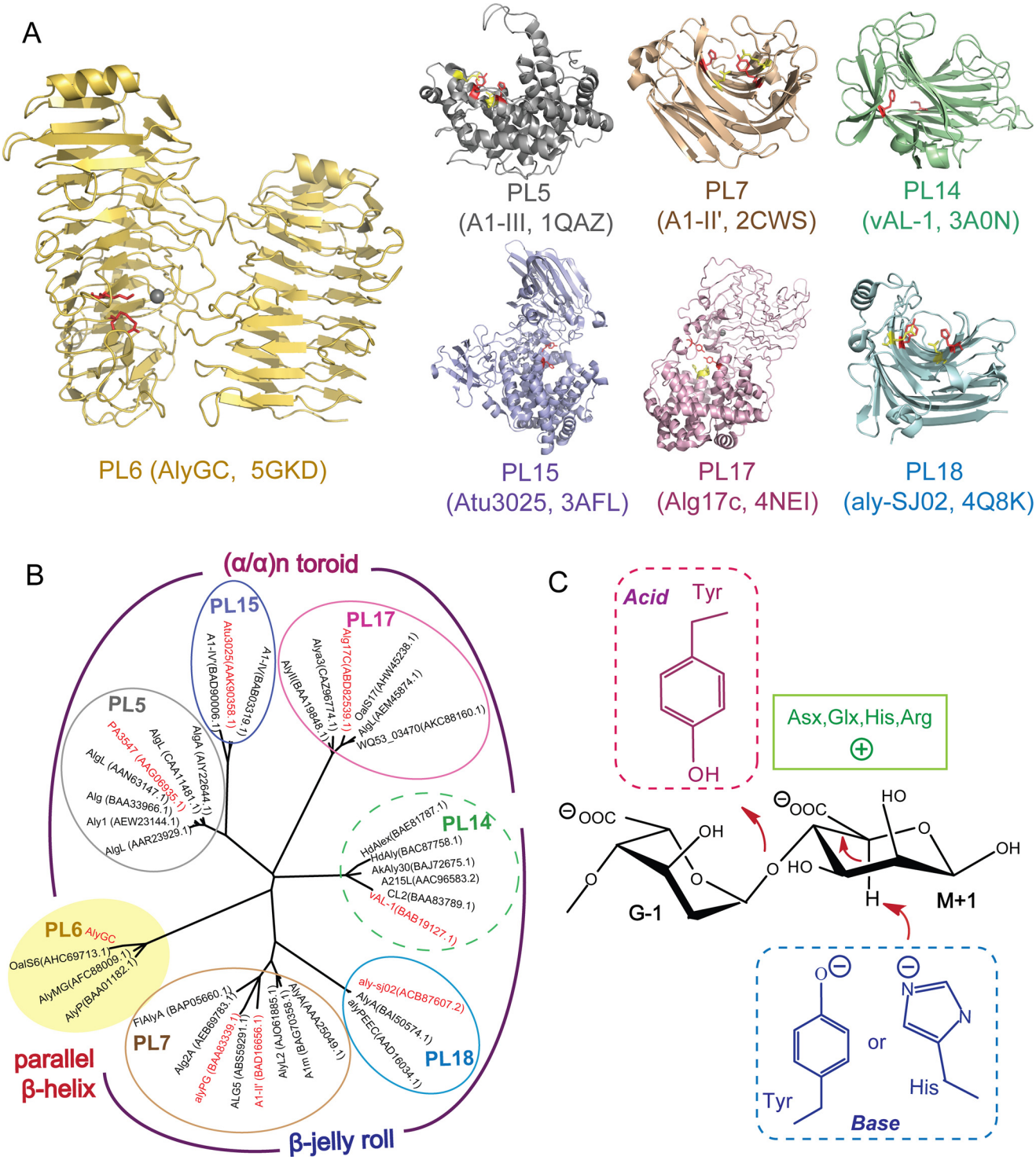

FIGURE 10. **Comparison of structures and catalytic mechanisms of alginate lyases.** *A,* overall structures of the alginate lyases in seven PL families. PL6 alginate lyase AlyGC (5GKD) is in *yellow*; PL5 alginate lyase AI-III (1QAZ) is in *gray*; PL7 alginate lyase AI–II′ (2CWS) is in *wheat*; PL14 alginate lyase vAL-1 (3A0N) is in *green*; PL15 alginate lyase Atu3025 (3AFL) is in *blue*; PL17 alginate lyase Alg17c (4NEI) is in *pink*, and PL18 alginate lyase aly-SJ02 (4Q8K) is in *cyan*. Brønsted acids and bases are shown as *red sticks*, and residues for neutralization are shown as *yellow sticks*. *B,* maximum likelihood tree of the characterized alginate lyases. PL14 alginate lyases *circled* with *dotted line* are from viruses or eukaryotes. Other lyases are from prokaryotes. One or two lyases with solved structures are shown in *red* as representatives in each family. *C,* schematic diagram of the histidine/tyrosine catalytic mechanisms of alginate lyases except for PL6 alginate lyases. Asx (Asp or Asn), Glx (Glu or Gln), His, or Arg neutralizes the acidic carboxyl group. Tyr functions as a Brønsted acid, and Tyr or His functions as a Brønsted base.

(Fig. 10*A*). A phylogenetic tree was constructed for the characterized alginate lyases in all the seven PL families, in which each family contains at least one alginate lyase with reported structure. Although alginate lyases are classified into seven PL families according to their primary structures, their three-dimensional structures can be grouped into 3-fold types. The alginate lyases from PL5, -15, and -17 adopt a $(\alpha/\alpha)_n$ toroid fold; those from PL7, -14, and -18 adopt a β-jelly roll fold, and AlyGC from

TABLE 1
Diffraction data and refinement statistics of WT-AlyGC, SeMet-AlyGC, and R241A-M4

Parameters	WT-AlyGC	SeMet-AlyGC	R241A-M4
Data collection			
Space group	*P* 1 21 1	*P* 1 21 1	*P* 21 21 21
Unit cell			
a, *b*, *c* (Å)[a]	116.6	116.3	82.7
	142.8	142.4	122.8
	126.2	125.6	195.3
α, β, γ (°)	90.0	90.0	90.0
	111.1	110.9	90.0
	90.0	90.0	90.0
Wavelength (Å)	0.9785	0.9785	0.9785
Resolution (Å)	50–2.19 (2.27–2.19)	50–2.80 (2.87–2.80)	50–2.56 (2.56–2.64)
Redundancy	4.6 (4.7)	6.9 (6.8)	5.5 (5.7)
Completeness (%)	98.6 (99.2)	98.1 (98.8)	98.0 (98.1)
R_{merge}[b]	0.124 (0.450)	0.141 (0.592)	0.141 (0.509)
Phasing			
Figure of merit[c]		0.348	
BAYES-CC		39.88	
Sites		45	
Refinement statistics			
Resolution (Å)	37.03–2.19 (2.27–2.19)		49.30–2.56 (2.66−2.56)
R_{work} (%)	16.6		19.1
R_{free} (%)	19.7		22.6
B-factor (Å^2)			
Protein	27.79		40.91
Solvent	34.66		40.76
Ligands	38.66		79.85
r.m.s.d. from ideal geometry			
r.m.s.d. length (Å)	0.009		0.012
r.m.s.d. angles (°)	1.130		1.130
Ramachandran Plot (%)[d]			
Favored	97.2		95.0
Allowed	2.6		4.6
Outliers	0.2		0.4

[a] Numbers in parentheses refer to data in the highest resolution shell.
[b] $R_{merge} = \Sigma_{hkl}\Sigma_i|I(hkl)_i - \langle I(hkl)\rangle|/\Sigma_{hkl}\Sigma_i \langle I(hkl)_i\rangle$.
[c] Probability-weighted average of the cosine of the phase error before and after density modification.
[d] The Ramachandran plot was calculated by PROCHECK program in CCP4i program package.

PL6 adopts a tandem parallel β-helix fold (Fig. 10, *A* and *B*). Thus, AlyGC of the PL6 family represents a new alginate lyase fold.

In addition, the catalytic mechanism of AlyGC is also significantly different from those of other alginate lyases. Previous studies showed that alginate lyases from the other families adopt the Tyr/His (Tyr) mechanism to catalyze a typical alkaline-induced β-elimination reaction. In the reaction, residues Asx (Asp/Asn), Glx (Glu/Gln), His, or Arg neutralize the negative charge of C5 carboxyl group to lower the pK_a of the C5 proton; a His (sometimes a Tyr) functions as the general base to attract the C5 proton, and a Tyr functions as the general acid to donate a proton to the O4 atom, thus forming a double bond between C4 and C5 (Fig. 10*C*) (8, 39). However, for AlyGC, a Ca^{2+}, rather than a residue, neutralizes the negative charge of C5 carboxyl group; a Lys acts as the base, and an Arg acts as the acid. Thus, AlyGC of the PL6 family adopts a catalytic mechanism different from that of the other families.

Experimental Procedures

Materials and Strains—Chondroitin sulfate B sodium salt from porcine intestinal mucosa and sodium alginate (viscosity, 15–20 cps) were purchased from Sigma. PolyM, polyG (6–8 kDa), and oligosaccharide substrates (purity ≥97%) were purchased from Zzstandard (China). Strain *G. chathamensis* S18K6^T was ordered from China General Microbiological Culture Collection Center (CGMCC) and grown in marine broth 2216 (BD Biosciences-Difco, America) at 20 °C. *E. coli* was cultured in Luria-Bertani (LB) medium at 37 °C.

Gene Cloning and Mutagenesis—The genome DNA of *G. chathamensis* S18K6^T was previously shotgun-sequenced and submitted to NCBI (GenBank^{TM} BAEM00000000.1). Gene (WP_007984897.1) (22) in this genome was deduced to encode a PL6 alginate lyase. This gene was named *alyGC* in this study. The *alyGC* gene was amplified from the genomic DNA of *G. chathamensis* S18K6^T via PCR and cloned into the vector pET-22b that contains a His tag. The residues encoding a putative signal peptide was predicted by the SignalP 4.1 Server. Site-directed and truncated mutations on AlyGC were conducted with the plasmid pET22b-*alyGC* as the template by using a QuikChange kit (Agilent Technologies).

Protein Expression and Purification—Recombinant proteins of WT AlyGC and its mutants were overexpressed in *E. coli* BL21 (DE3) and cultured at 20 °C for 16 h in LB broth containing 100 μg/ml ampicillin under the induction of 0.3 mM isopropyl β-D-1-thiogalactopyranoside (IPTG). Selenomethionine (SeMet)-labeled AlyGC was expressed by inhibiting endogenous methionine biosynthesis in *E. coli* BL21 (DE3) in defined media (40). Cells grown overnight in LB medium were harvested and inoculated in the M9 medium containing 100 mg/liter lysine, phenylalanine, and threonine, 50 mg/liter isoleucine, leucine, and valine, 5.2% (w/v) glucose, and 0.65% (w/v) yeast nitrogen base (YNB), which was then cultured at 37 °C. When the A_{600} reached 0.6, the culture was cooled to

15 °C and 50 mg/liter L-SeMet was added. Fifteen min later, the culture was incubated at 15 °C for 14 h under the induction of 0.4 mM IPTG.

The recombinant proteins were first purified by nickel-nitrilotriacetic acid resin (Qiagen, Germany) and then fractionated by anion exchange on a Source 15Q column (GE Healthcare) and gel filtration on a Superdex G-200 column (GE Healthcare). Aldolase (158 kDa), conalbumin (75 kDa), and ovalbumin (43 kDa) from GE Healthcare were used as protein size standards.

Biochemical Characterization of AlyGC—Protein concentration was determined with bovine serum albumin as the standard by using a BCA protein assay kit (Thermo Fisher Scientific). The activities of WT AlyGC and its mutants toward alginate and PG were measured by the ultraviolet absorption spectrometry method (7, 41). Briefly, a 200-μl mixture containing 25 μg/ml enzyme and 2 mg/ml substrate in 50 mM Tris-HCl (pH 7.5) was incubated at 30 °C for 30 min. After that, the reaction mixture was boiled for 10 min to terminate the reaction. Then an increase in the absorbance at 235 nm (A_{235}) caused by the production of unsaturated uronic in the mixture was monitored. One unit of enzyme activity was defined as the amount of enzyme needed to produce an A_{235} increase of 0.1 per min. The enzyme assays toward DS were performed with the method described by Michel *et al.* (26). The action mode of AlyGC was measured by TLC using PG as the substrate. Monoguluronic acid standard and the product were separated using a solvent system of 1-butanol/acetic acid/water (4:6:1, v/v) and visualized by heating TLC plates at 90 °C for 15 min after spraying with 10% (v/v) sulfuric acid in ethanol.

The ion in AlyGC molecule was investigated by using ICP-OES (42). To determine the effect of EDTA on the activity of AlyGC, EDTA at different concentrations was added to the reaction mixtures containing 3.5 μg/ml enzyme and 2 mg/ml PG in 50 mM Tris-HCl (pH 7.5) before the enzyme activity was determined. Apo-AlyGC was prepared by the addition of 2 mM EDTA and subsequent desalination. The recovered activity of apo-AlyGC was measured after Ca^{2+}, Mg^{2+}, or Mn^{2+} was added. Ca^{2+} was added in the final concentrations of 0.05, 0.1, 0.15, and 0.2 mM. Mg^{2+} or Mn^{2+} was added in the final concentration of 0.2 mM. Enzyme activity was determined by measuring the absorbance of the mixture at 548 nm with the thiobarbituric acid (TBA) method (43). One unit of enzyme activity was defined as the amount of enzyme required to liberate 1 nmol of β-formylpyruvic acid per min at 30 °C.

Crystallization and Data Collection—WT AlyGC (15 mg/ml) was crystallized at 20 °C by the sitting drop method in the buffer containing 25% (w/v) polyethylene glycol (PEG) 1500 and 100 mM SPG (succinic acid, sodium dihydrogen phosphate, and glycine) (pH 8.5). Crystals of SeMet-AlyGC (10 mg/ml) were grown in the buffer containing 200 mM malonate sodium (pH 7.0) and 18% (w/v) PEG 3350. The inactive mutant R241A (10 mg/ml) mixed with M4 at a molar ratio of 1:15 was crystallized at 20 °C by the hanging drop method in the buffer containing 100 mM HEPES-NaOH (pH 7.3), 8% ethylene glycol, and 11% PEG 8000. X-ray diffraction data were collected on BL17U1 beam line at the Shanghai Synchrotron Radiation Facility using detector ADSC Quantum 315r (44). The initial diffraction data sets were processed by HKL2000 (45). Data collection statistics are shown in Table 1.

Structure Determination and Refinement—Heavy atoms were searched by SHELXD (46). The phase problems were solved by single-wavelength anomalous diffraction (SAD) method using Phenix program Autosol (47). Initial model building was finished by Phenix program AutoBuild (47). Refinement of the AlyGC structure was done by Phenix program Refine (47) and Coot (48) alternately. The quality of the final model is summarized in Table 1. All the structure figures were processed using the program PyMOL.

Dynamic Light Scattering and Circular Dichroism Spectra—The DLS experiment was performed on Dynapro Titan TC (Wyatt Technology) at 4 °C using 5.7 mg/ml AlyGC in a buffer containing 10 mM Tris-HCl (pH 8.0) and 100 mM NaCl, and analyses were done by Dynamics 7.1.0 software. CD spectra were collected from 250 to 200 nm at a scan speed of 200 nm/min with a path length of 0.1 cm on a J-810 spectropolarimeter (Jasco, Japan) at 25 °C. The final concentration of the proteins for CD spectra was 2.5 μM in 10 mM Tris-HCl (pH 7.5).

Author Contributions—F. X. and F. D. performed all experiments. X. C. directed the experiments. F. X. and X. C. wrote the manuscript. P. W. and H. C. solved the structures. C. L. and P. L. analyzed the data. Y. Z. and X. C. designed the research. X. P. edited the manuscript.

Acknowledgments—We thank the staff of BL17U1 beamline at National Center for Protein Sciences Shanghai and Shanghai Synchrotron Radiation Facility, Shanghai, People's Republic of China, for assistance during data collection.

References

1. Duarte, C. M., Middelburg, J. J., and Caraco, N. (2005) Major role of marine vegetation on the oceanic carbon cycle. *Biogeosci. Discs.* **2,** 1–8
2. Popper, Z. A., Michel, G., Hervé, C., Domozych, D. S., Willats, W. G., Tuohy, M. G., Kloareg, B., and Stengel, D. B. (2011) Evolution and diversity of plant cell walls: from algae to flowering plants. *Annu. Rev. Plant Biol.* **62,** 567–590
3. Haug, A., Larsen, B., Smidsrød, O., Eriksson, G., Blinc, R., Paušak, S., Ehrenberg, L., and Dumanović, J. (1967) Studies on the sequence of uronic acid residues in alginic acid. *Acta Chem. Scand.* **21,** 691–704
4. Smidsrod, O., and Draget, K. I. (1996) Chemistry and physical properties of alginates. *Carbohydr. Eur.* **14,** 6–13
5. Lee, K. Y., and Mooney, D. J. (2012) Alginate: properties and biomedical applications. *Prog. Polym. Sci.* **37,** 106–126
6. Wong, T. Y., Preston, L. A., and Schiller, N. L. (2000) ALGINATE LYASE: review of major sources and enzyme characteristics, structure-function analysis, biological roles, and applications. *Annu. Rev. Microbiol.* **54,** 289–340
7. Dong, S., Wei, T. D., Chen, X. L., Li, C. Y., Wang, P., Xie, B. B., Qin, Q. L., Zhang, X. Y., Pang, X. H., Zhou, B. C., and Zhang, Y. Z. (2014) Molecular insight into the role of the N-terminal extension in the maturation, substrate recognition, and catalysis of a bacterial alginate lyase from polysaccharide lyase family 18. *J. Biol. Chem.* **289,** 29558–29569
8. Zhu, B., and Yin, H. (2015) Alginate lyase: Review of major sources and classification, properties, structure-function analysis and applications. *Bioengineered* **6,** 125–131
9. Li, L., Jiang, X., Guan, H., and Wang, P. (2011) Preparation, purification and characterization of alginate oligosaccharides degraded by alginate lyase from *Pseudomonas* sp. HZJ 216. *Carbohydr. Res.* **346,** 794–800

10. Inoue, A., Mashino, C., Kodama, T., and Ojima, T. (2011) Protoplast preparation from *Laminaria japonica* with recombinant alginate lyase and cellulase. *Mar. Biotechnol.* **13,** 256–263
11. Islan, G. A., Bosio, V. E., and Castro, G. R. (2013) Alginate lyase and ciprofloxacin co-immobilization on biopolymeric microspheres for cystic fibrosis treatment. *Macromol. Biosci.* **13,** 1238–1248
12. Hatch, R. A., and Schiller, N. L. (1998) Alginate lyase promotes diffusion of aminoglycosides through the extracellular polysaccharide of mucoid *Pseudomonas aeruginosa*. *Antimicrob. Agents Chemother.* **42,** 974–977
13. Preiss, J., and Ashwell, G. (1962) Alginic acid metabolism in bacteria. I. Enzymatic formation of unsaturated oligosaccharides and 4-deoxy-L-*erythro*-5-hexoseulose uronic acid. *J. Biol. Chem.* **237,** 309–316
14. Doubet, R. S., and Quatrano, R. S. (1984) Properties of alginate lyases from marine bacteria. *Appl. Environ. Microbiol.* **47,** 699–703
15. Park, D., Jagtap, S., and Nair, S. K. (2014) Structure of a PL17 family alginate lyase demonstrates functional similarities among exotype depolymerases. *J. Biol. Chem.* **289,** 8645–8655
16. Brown, B. J., and Preston, J. F., 3rd (1991) L-Guluronan-specific alginate lyase from a marine bacterium associated with *Sargassum*. *Carbohydr. Res.* **211,** 91–102
17. Nakada, H. I., and Sweeny, P. C. (1967) Alginic acid degradation by eliminases from abalone hepatopancreas. *J. Biol. Chem.* **242,** 845–851
18. Cantarel, B. L., Coutinho, P. M., Rancurel, C., Bernard, T., Lombard, V., and Henrissat, B. (2009) The carbohydrate-active EnZymes database (CAZy): an expert resource for glycogenomics. *Nucleic Acids Res.* **37,** D233–D238
19. Yoon, H. J., Mikami, B., Hashimoto, W., and Murata, K. (1999) Crystal structure of alginate lyase A1-III from *Sphingomonas* species A1 at 1.78 A resolution. *J. Mol. Biol.* **290,** 505–514
20. Yamasaki, M., Moriwaki, S., Miyake, O., Hashimoto, W., Murata, K., and Mikami, B. (2004) Structure and function of a hypothetical *Pseudomonas aeruginosa* protein PA1167 classified into family PL-7: a novel alginate lyase with a β-sandwich fold. *J. Biol. Chem.* **279,** 31863–31872
21. Ogura, K., Yamasaki, M., Yamada, T., Mikami, B., Hashimoto, W., and Murata, K. (2009) Crystal structure of family 14 polysaccharide lyase with pH-dependent modes of action. *J. Biol. Chem.* **284,** 35572–35579
22. Ochiai, A., Yamasaki, M., Mikami, B., Hashimoto, W., and Murata, K. (2010) Crystal structure of exotype alginate lyase Atu3025 from *Agrobacterium tumefaciens*. *J. Biol. Chem.* **285,** 24519–24528
23. Maki, H., Mori, A., Fujiyama, K., Kinoshita, S., and Yoshida, T. (1993) Cloning, sequence analysis and expression in *Escherichia coli* of a gene encoding an alginate lyase from *Pseudomonas* sp. OS-ALG-9. *J. Gen. Microbiol.* **139,** 987–993
24. Lee, S. I., Choi, S. H., Lee, E. Y., and Kim, H. S. (2012) Molecular cloning, purification, and characterization of a novel polyMG-specific alginate lyase responsible for alginate MG block degradation in *Stenotrophomas maltophilia* KJ-2. *Appl. Microbiol. Biotechnol.* **95,** 1643–1653
25. Li, S., Wang, L., Han, F., Gong, Q., and Yu, W. (2016) Cloning and characterization of the first polysaccharide lyase family 6 oligoalginate lyase from marine *Shewanella* sp. Kz7. *J. Biochem.* **159,** 77–86
26. Michel, G., Pojasek, K., Li, Y., Sulea, T., Linhardt, R. J., Raman, R., Prabhakar, V., Sasisekharan, R., and Cygler, M. (2004) The structure of chondroitin B lyase complexed with glycosaminoglycan oligosaccharides unravels a calcium-dependent catalytic machinery. *J. Biol. Chem.* **279,** 32882–32896
27. Huang, W., Matte, A., Li, Y., Kim, Y. S., Linhardt, R. J., Su, H., and Cygler, M. (1999) Crystal structure of chondroitinase B from *Flavobacterium heparinum* and its complex with a disaccharide product at 1.7 A resolution. *J. Mol. Biol.* **294,** 1257–1269
28. Qin, Q. L., Xie, B. B., Yu, Y., Shu, Y. L., Rong, J. C., Zhang, Y. J., Zhao, D. L., Chen, X. L., Zhang, X. Y., Chen, B., Zhou, B. C., and Zhang, Y. Z. (2014) Comparative genomics of the marine bacterial genus *Glaciecola* reveals the high degree of genomic diversity and genomic characteristic for cold adaptation. *Environ. Microbiol.* **16,** 1642–1653
29. Matsuyama, H., Hirabayashi, T., Kasahara, H., Minami, H., Hoshino, T., and Yumoto, I. (2006) *Glaciecola chathamensis* sp. nov., a novel marine polysaccharide-producing bacterium. *Int. J. Syst. Evol. Microbiol.* **56,** 2883–2886
30. Pickersgill, R., Jenkins, J., Harris, G., Nasser, W., and Robert-Baudouy, J. (1994) The structure of *Bacillus subtilis* pectate lyase in complex with calcium. *Nat. Struct. Biol.* **1,** 717–723
31. Alahuhta, M., Chandrayan, P., Kataeva, I., Adams, M. W., Himmel, M. E., and Lunin, V. V. (2011) A 1.5 A resolution X-ray structure of the catalytic module of *Caldicellulosiruptor bescii* family 3 pectate lyase. *Acta Crystallogr. Sect. F Struct. Biol. Cryst. Commun.* **67,** 1498–1500
32. Jenkins, J., Shevchik, V. E., Hugouvieux-Cotte-Pattat, N., and Pickersgill, R. W. (2004) The crystal structure of pectate lyase Pel9A from *Erwinia chrysanthemi*. *J. Biol. Chem.* **279,** 9139–9145
33. Jenkins, J., and Pickersgill, R. (2001) The architecture of parallel β-helices and related folds. *Prog. Biophys. Mol. Biol.* **77,** 111–175
34. Jenkins, J., Mayans, O., and Pickersgill, R. (1998) Structure and evolution of parallel β-helix proteins. *J. Struct. Biol.* **122,** 236–246
35. Holm, L., and Rosenström, P. (2010) Dali server: conservation mapping in 3D. *Nucleic Acids Res.* **38,** W545–W549
36. Rozeboom, H. J., Bjerkan, T. M., Kalk, K. H., Ertesvåg, H., Holtan, S., Aachmann, F. L., Valla, S., and Dijkstra, B. W. (2008) Structural and mutational characterization of the catalytic A-module of the mannuronan C-5-epimerase AlgE4 from *Azotobacter vinelandii*. *J. Biol. Chem.* **283,** 23819–23828
37. Thompson, J. E., Pourhossein, M., Waterhouse, A., Hudson, T., Goldrick, M., Derrick, J. P., and Roberts, I. S. (2010) The K5 lyase KflA combines a viral tail spike structure with a bacterial polysaccharide lyase mechanism. *J. Biol. Chem.* **285,** 23963–23969
38. Davies, G. J., Wilson, K. S., and Henrissat, B. (1997) Nomenclature for sugar-binding subsites in glycosyl hydrolases. *Biochem. J.* **321,** 557–559
39. Ertesvåg H. (2015) Alginate-modifying enzymes: biological roles and biotechnological uses. *Front. Microbiol.* **6,** 523
40. Doublié, S. (2007) Production of selenomethionyl proteins in prokaryotic and eukaryotic expression systems. *Methods Mol. Biol.* **363,** 91–108
41. Thomas, F., Lundqvist, L. C., Jam, M., Jeudy, A., Barbeyron, T., Sandström, C., Michel, G., and Czjzek, M. (2013) Comparative characterization of two marine alginate lyases from *Zobellia galactanivorans* reveals distinct modes of action and exquisite adaptation to their natural substrate. *J. Biol. Chem.* **288,** 23021–23037
42. Wang, P., Chen, X. L., Li, C. Y., Gao, X., Zhu, D. Y., Xie, B. B., Qin, Q. L., Zhang, X. Y., Su, H. N., Zhou, B. C., Xun, L. Y., and Zhang, Y. Z. (2015) Structural and molecular basis for the novel catalytic mechanism and evolution of DddP, an abundant peptidase-like bacterial Dimethylsulfoniopropionate lyase: a new enzyme from an old fold. *Mol. Microbiol.* **98,** 289–301
43. Weissbach, A., and Hurwitz, J. (1959) The formation of 2-keto-3-deoxyheptonic acid in extracts of *Escherichia coli* B. I. Identification. *J. Biol. Chem.* **234,** 705–709
44. Wang, Z., Pan, Q., Yang, L., Zhou, H., Xu, C., Yu, F., Wang, Q., Huang, S., and He, J. (2016) Automatic crystal centering procedure at the SSRF macromolecular crystallography beamline. *J. Synchrotron Radiat.* **23,** 1323–1332
45. Ducruix, A., and Giegé, R. (eds) (1999) *Crystallization of Nucleic Acids and Proteins,* 2nd Ed., pp. 391–419, Oxford University Press, New York
46. Schneider, T. R., and Sheldrick, G. M. (2002) Substructure solution with SHELXD. *Acta Crystallogr. D Biol. Crystallogr.* **58,** 1772–1779
47. Adams, P. D., Grosse-Kunstleve, R. W., Hung, L. W., Ioerger, T. R., McCoy, A. J., Moriarty, N. W., Read, R. J., Sacchettini, J. C., Sauter, N. K., and Terwilliger, T. C. (2002) PHENIX: building new software for automated crystallographic structure determination. *Acta Crystallogr. D Biol. Crystallogr.* **58,** 1948–1954
48. Emsley, P., and Cowtan, K. (2004) Coot: model-building tools for molecular graphics. *Acta Crystallogr. D Biol. Crystallogr.* **60,** 2126–2132